Biomass Conversion and Biorefinery (2023) 13:8701–8712
https://doi.org/10.1007/s13399-020-01164-4

ORIGINAL ARTICLE

Biohydrogen production from photodecomposition of various cellulosic biomass wastes using metal-TiO_2 catalysts

Syaahidah Abdul Razak[1] · Abdul Hanif Mahadi[1] · Rosnah Abdullah[1] · Hartini Mohd Yasin[2] · Fairuzeta Ja'afar[2] · Norizah Abdul Rahman[3] · Hasliza Bahruji[1]

Received: 15 August 2020 / Revised: 15 November 2020 / Accepted: 18 November 2020 / Published online: 27 November 2020

Abstract

Biohydrogen generation from direct photocatalytic decomposition of lignocellulose biomass waste was investigated using TiO_2 with metal co-catalysts. The behavior of the photocatalyst was explored by studying the effect of metal co-catalysts (Pd, Cu, Ni, Ce) and the amount of metal loading. The reactivity of TiO_2 was found to vary depending on the metal co-catalysts, with the order of reactivity being Pd > Cu > Ni = Ce. Cellulose samples extracted from coconut husk, fern fiber, and cotton linter were characterized using XRD, FTIR, and SEM analysis. Crystallinity index (CI), degree of polymerization (DP), and α-cellulose and hemicellulose concentrations were correlated with hydrogen yield. Cotton linter cellulose with high CI and DP produced 131 μmol of H_2 in 3 h followed by cellulose extracted from coconut husk at 38 μmol and fern fibers at 6 μmol. High concentrations of hemicellulose enhanced the rate of H_2 production due to the release of acetic acid during photodecomposition and accelerated the hydrolysis. Sugar fractions containing glucose and fructose obtained from hydrothermal treatment of cotton linter cellulose improved H_2 yield, which suggests that the rate limiting step of the reaction is the dissociation of β(1→4)-glycosidic bonds to form sugar monomers.

Keywords Cellulose · Holocellulose · Sugar · Hydrogen · Pd/TiO_2 · Photocatalysis · Biomass

1 Introduction

Conversion of biomass into renewable green energy is seen as an alternative substitute to the depleting fossil fuel resources. Cellulose and hemicellulose consist of carbon, hydrogen, and oxygen atoms in the form of linear polymeric saccharides chains but with varying homogeneity [1]. Cellulose is synthesized by living organisms, particularly plants, as the main substance in the cell wall [2]. As the most abundant organic compound, conversion of cellulose to value-added commodities has been investigated, for example as an additive in food and pharmaceutical industries [3]. Conversion of cellulose into glucose using methods such as hydrothermal treatment and hydrolysis also showed promising routes for conversion of cellulose to value-added commodities [4, 5]. Hydrothermal degradation of cellulose using subcritical water at 200–300 °C produced sugar monomers, in particular glucose and fructose [6]. Cellulose has also been investigated as alternative biomass for sustainable generation of H_2 gas via high-temperature pyrolysis [7]. Pyrolysis required high-temperature decomposition of cellulose that produced H_2 and various gasses such as CO_2, CH_4, and C_2-C_4 hydrocarbons [8]. High-temperature decomposition of cellulose also further converted cellulose to volatile organic compounds and char [9]. Conversion of cellulose to hydrogen at low temperatures can be carried out using methods such as dark fermentation [10, 11], photocatalysis [12, 13], and electrolysis [14, 15]. In all these methods, decomposition of cellulose occurred through random dissociation of β(1→4)-glycosidic bonds with 172 ± 2 kJ/mol of activation energy [16]. Dark fermentation has been extensively investigated as environmental friendly route for biohydrogen production from

✉ Hasliza Bahruji
hasliza.bahruji@ubd.edu.bn

[1] Centre of Advanced Materials and Energy Sciences, Universiti Brunei Darussalam, Jalan Tungku Link, Gadong, Bandar Seri Begawan BE1410, Brunei

[2] Chemical Sciences Programme, Faculty of Science, Universiti Brunei Darussalam, Jalan Tungku Link, Gadong, Bandar Seri Begawan BE1410, Brunei

[3] Department of Chemistry, Faculty of Science, Universiti Putra Malaysia, 43400 Serdang, Selangor, Malaysia

biomass waste [17]. The efficiency of H_2 production depends on temperature, pH, and the ability of microorganism to break down carbohydrate into hydrogen [18]. However, dark fermentation often requires a long fermentation time to produce high yield of H_2 [18, 19]. Biohydrogen production from electrolysis of lignocellulosic biomass exhibited high efficiency when using cellulose in comparison to holocellulose and lignin [14]; however, this method used-Pt based electrode and requires high energy consumption [20].

Photocatalysis provides a sustainable route for H_2 gas generation at ambient conditions while taking the full advantage of energy from sunlight. Quantum efficiency of photocatalytic hydrogen production from methanol reforming while using Pd/TiO_2 catalysts was higher in UV-B region at ~35% efficiency [21]. Photocatalytic decomposition of lignocellulosic biomass is another feasible and practical route with much higher efficiency in comparison to direct photocatalytic water splitting, with potential to store up to 12% of the light energy [22]. Cellulose becomes a sacrificial agent during photocatalytic water spitting, which degrades to produce CO_2, thus allowing photoreduction of water for H_2 production [12]. Studies on simultaneous cellulose conversion and hydrogen production using TiO_2 photocatalysts suggest the feasibility of the process to utilize readily available biomass materials for isolating H_2 from water [23]. Apart from acid hydrolysis, the ball milling method was also used to initiate cellulose decomposition into its glucose unit, which enhanced the photocatalytic decomposition of cellulose [24]. Formic acid and glucose, identified as intermediates [23], also decomposed in the photoreforming reaction to form CO_2 and H_2 gasses [25] on a variety of photocatalysts such as Pt/TiO_2 [26], Pd/TiO_2 [27], and other noble metals [28].

This research aimed to investigate sustainable H_2 gas production from cellulose derived from biomass waste via photocatalysis. Cellulose isolated from coconut husk, fern fiber, and cotton linter with different crystallinity and degree of polymerization will be used to elucidate the effects of cellulose properties towards H_2 production. H_2 production will also be correlated with the composition of hemicellulose and α-cellulose. Photodecomposition of cellulose was carried out using Pd-, Cu-, Ni-, and Ce-loaded TiO_2 photocatalysts. Finally, aqueous solutions containing glucose and fructose obtained from hydrothermal treatment of cellulose were also investigated for H_2 production in order to provide insights into the mechanism of the reaction.

2 Experimental details

2.1 Materials

Commercial TiO_2 used in this study was supplied by Sigma-Aldrich. Metal precursors such as copper (II) nitrate hydrate ($Cu(NO_3)_2{\cdot}H_2O$, EMSURE), potassium tetrachloropalladate (K_2PdCl_4, Sigma-Aldrich), cerium nitrate hexahydrate ($Ce(NO_3)_3{\cdot}6H_2O$, EMSURE), and nickel nitrate hexahydrate ($Ni(NO_3)_2{\cdot}6H_2O$, EMSURE) were used to prepare metal/TiO_2 catalysts. Cotton linter cellulose (medium fibers, 99.98%) was supplied by Sigma-Aldrich.

2.2 Preparation of catalysts

Incipient wetness impregnation method was used to prepare metal/TiO_2 photocatalysts based on previously reported work that indicated high photocatalytic activity was achieved compared to the colloidal method [29]. The required amount of metal precursor at 0.3% of metal weight was dissolved in a small amount of water before being added to TiO_2. The mixture was further ground until it formed a paste. Afterwards, the paste was dried at 120 °C for 2 h followed by calcination at 550 °C for 3 h.

2.3 Characterization studies

X-ray diffraction (XRD, Shimadzu) was used to determine the phase composition and analyze crystal structure of the samples. The patterns were recorded in the 2θ within range of 10 to 60° using a radiation source of λ = 1.54 Å at 40 kV and 30 mA. The crystallinity index (CI) of cellulose was calculated using equation below [26, 30]:

$$\mathrm{CI}\,(\%) = \frac{\mathrm{I}_{200} \times \mathrm{I}_{\mathrm{AM}}}{\mathrm{I}_{200}} \times 100 \quad (1)$$

where I_{002} represents the maximum intensity of the (200) plane diffraction peak at 2θ = 23.1° and I_{AM} represents the minimum intensity between (110) and (200) diffraction peak at 2θ = 19.0° [26, 30, 31]. The morphology of the samples was studied using JEOL scanning electron microscopy (SEM) equipped with energy dispersive X-ray (EDX). Surface area, pore volume, and pore size measurements were carried out by N_2 adsorption-desorption at 77 K (Micromeritics ASAP 2020). Fourier-transform infrared spectroscopy (FTIR, CARY 630) was employed to determine the presence of functional group in the cellulose isolated from coconut husk, fern fiber, and cotton linter. All FTIR spectra were measured at 650–4000 cm^{-1} in transmittance mode. UV-Vis spectroscopy (CARY 3000) was used to study the optical absorption properties of the catalysts. The spectra were recorded at room temperature using wavelength from 200 to 800 nm.

2.4 Cellulose isolation from coconut husk and fern fiber

Holocellulose and alpha-cellulose were isolated from two raw biomass wastes, namely Malayan tall coconut (*Cocos nucifera*

L.) husks and fern fiber (*Dicranopteris linearis*), using the "wood industry" method. The "wood industry" method is a standard method provided by the Technical Association of the Pulp and Paper Industry (TAPPI) that allowed efficient removal of lignin for extraction of cellulose [32–34]. The method is also known as acid-chlorite treatment. Raw biomass materials were collected and sun-dried for 2 weeks. Dried materials were cut to 2–3 cm, ground using a kitchen blender, and sieved using 212-μm sieve. The raw materials were then treated using Soxhlet extraction in acetone for 16 h. For holocellulose (a mixture of α-cellulose and hemicellulose) extraction using sodium chlorite, 4 g of extractive-free residue was treated with 160 cm^3 0.2 M sodium acetate solution and heated to 75 °C for 5 h, followed by the addition of 4 cm^3 of 20% (w/v) sodium chlorite. The mixture was then cooled, filtered, and washed with distilled water and acetone. The residue was then oven-dried at 105 °C. The dried residue (holocellulose) was further treated with sodium hydroxide to remove the remaining hemicellulose content. To obtain cellulose, 1 g of the extracted holocellulose was added to 20 cm^3 17.5% (w/v) sodium hydroxide solution at room temperature for 30 min. The mixture was washed and filtered twice with 40 ml of distilled water followed by 3 ml of 10% (w/v) acetic acid solution, and finally with 100 ml of hot water. The residue (cellulose) was then oven-dried at 105 °C.

2.5 Determination of degree of polymerization of cellulose

The viscosities of the cellulose samples were measured by using 0.5 M cupriethethylenediamine (CUEN) according to TAPPI method in a Cannon Fenske capillary viscometer. The viscosity average DP of the cellulose samples was calculated from the intrinsic viscosity [η] according to Eq. 2 [35]:

$$DP^{0.905} = 0.75[\eta] \quad (2)$$

2.6 Hydrothermal decomposition of cellulose

The conversion of cellulose to glucose and fructose was carried out using cellulose cotton linter and water mixture using hydrothermal reaction at 10 MPa and 250 and 270 °C for 15 min. At the end of 15 min, the reactor was cooled down immediately to terminate all reactions. The water-soluble products were filtered off from the cellulose residues using 0.45 μm membranes and analyzed using gas chromatography–mass spectrometry (GC-MS).

2.7 Photocatalytic H_2 production

Photocatalytic H_2 production was carried out in a 60-ml glass bottle equipped with a rubber septum for gas sampling. Fifty milligrams of photocatalyst and 0.1 g of cellulose cotton linter were suspended in 30 ml of distilled water and placed in an irradiation chamber BS-02 in which the interior was surrounded by mirrors, employing three MH-lamps of 150 W for UVA-visible light simulation. The suspension was stirred for 10 min to ensure homogeneous catalyst dispersion. Prior to light irradiation, the reaction mixture was purged with nitrogen gas for the removal of air and degassing of the solution. Afterwards, the light source was switched on and the mixture was stirred continuously for 3 h under light irradiation. The gas sample (3 ml) was collected at 30-min interval from the reactor and analyzed using gas chromatography (GC-2014, Shimadzu), where argon was used as carrier gas. The procedure was repeated three times to get the average yield of H_2 and the standard deviation. The photocatalytic reaction outlined above was also carried out on an aqueous sugar solution derived from hydrothermal decomposition of cellulose cotton linter for comparison.

3 Results and discussion

3.1 Characterization of the catalysts

Figure 1 shows the XRD patterns of TiO_2 and metal deposited onto TiO_2. All catalysts exhibited high crystalline anatase structure peaks at 25.4°, 37.1°, 37.9°, 38.6°, 48.1°, 54.4°, and 55.2°. Furthermore, the patterns also showed comparatively small peaks ascribed to rutile structure [36, 37]. The peaks corresponding to the metals—Pd, Cu, Ce, and Ni—were not observed from XRD due to the formation of highly dispersed metal nanoparticles on TiO_2 support [38]. The

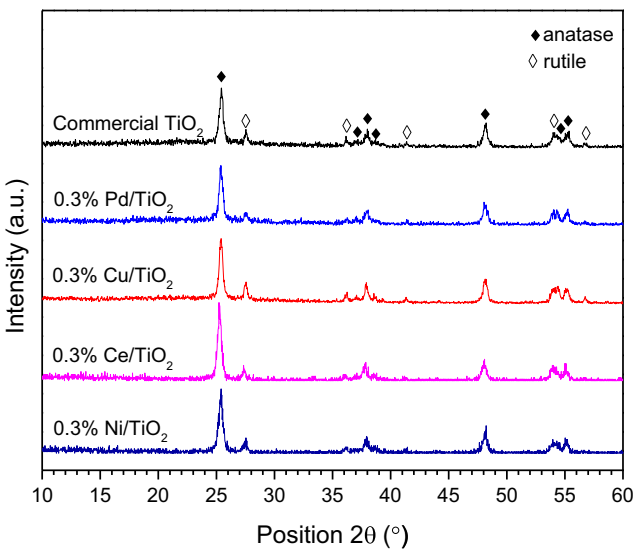

Fig. 1 XRD patterns of commercial TiO_2, 0.3% Pd/TiO_2, 0.3% Cu/TiO_2, 0.3% Ce/TiO_2, and 0.3% Ni/TiO_2

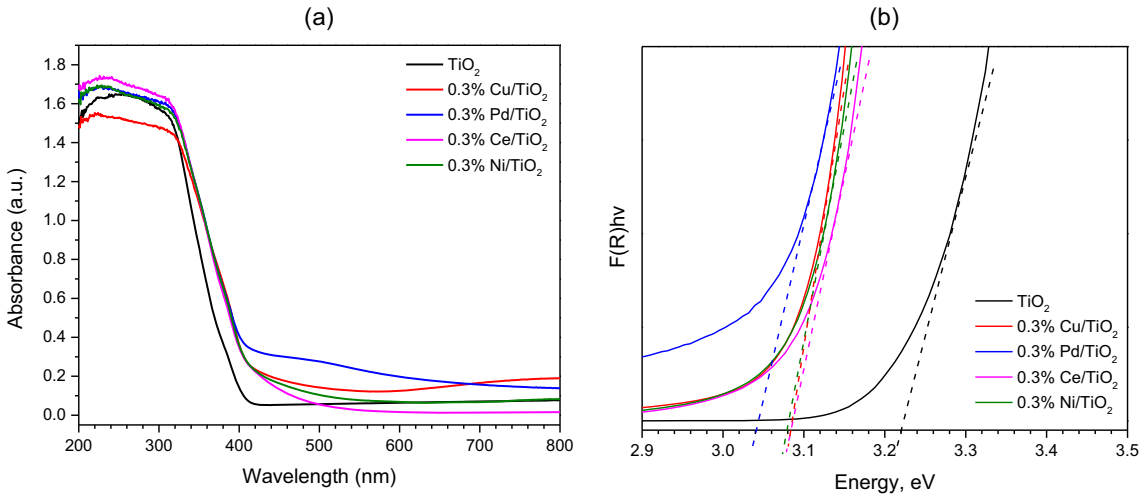

Fig. 2 (a) Diffuse reflectance UV-Vis absorption spectra of the photocatalysts. (b) Kubelka-Munk plot for the estimation of the band gap energies of the photocatalysts

structure of TiO_2 did not show any significant changes following impregnation with metal co-catalysts.

Diffuse reflectance UV-Vis spectra of TiO_2 in Fig. 2 showed the absorbance band edges of TiO_2 were observed at 350 to 400 nm, corresponding to the band gap at approximately ~3.22 eV. Following impregnation with metal nanoparticles, the band gap of the catalyst was slightly reduced to 3.0 and 3.1 eV. Cu/TiO_2 and Pd/TiO_2 also showed additional absorption bands in visible region. Cu/TiO_2 exhibited a broad absorption peak at 600–800 nm whereas Pd/TiO_2 only showed a discrete absorption peak around 400–550 near UV region. The observation was correlated with the ability of the electron on the surface of metallic nanoparticles to oscillate during excitation with incident radiation, which is also known as localized surface plasmon resonance (LSPR) [39]. However, the plasmonic resonance was not observed on Ni and Ce. N_2 analysis of the catalysts following deposition of metal onto TiO_2 indicated the surface area of TiO_2 was reduced from 47 m^2/g to 41 m^2/g after impregnation with Pd. Similar observation was also found when Ni was added to give 42 m^2/g. Impregnation with Cu further reduced the surface area to 38 m^2/g. On the other hand, Ce/TiO_2 only showed slight reduction to give 45 m^2/g of surface area. It is interesting to note that at the same loading content, all metal/TiO_2 combinations showed different surface areas, presumably due to the differences in metal dispersion on TiO_2.

Figure 3(a) displays the surface morphology of Pd/TiO_2 catalysts analyzed using SEM. Spherical shape agglomeration with relatively uniform sizes was analyzed on Pd/TiO_2 catalyst. Similar aggregations of spherical nanoparticles were observed for TiO_2 and Cu/TiO_2 catalysts (Fig. S1 and Fig. S2). EDX analysis also showed the elemental mapping images of

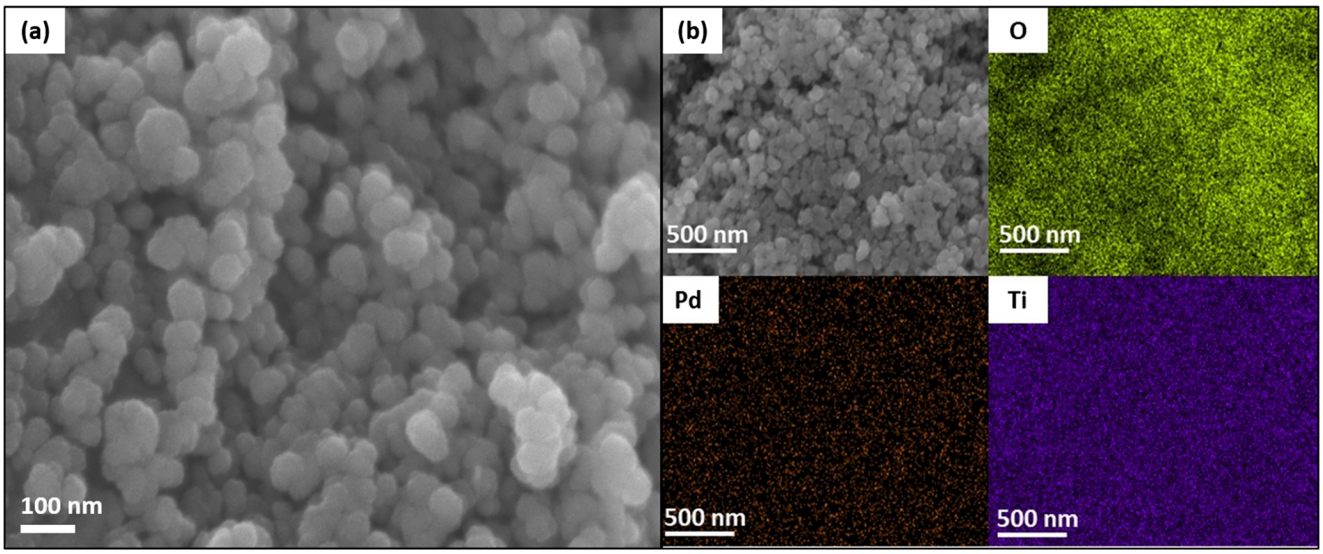

Fig. 3 (a) SEM images Pd/TiO_2. (b) Elemental mapping of /TiO_2 photocatalysts

investigated components in the samples, as shown in Fig. 3(b). Analysis of each element showed even and uniform distributions of Pd, Ti, and O across the TiO_2 surface. This is further evidence of the presence of metal co-catalysts on TiO_2 and confirmed that the incipient-wetness impregnation method provides a good dispersion of metal throughout the TiO_2 surface.

3.2 Characterization of cellulose

3.2.1 XRD analysis of cellulose

Cellulose samples from coconut husk, fern, and cotton linter were characterized using XRD analysis (Fig. 4). XRD patterns of cellulose cotton linter showed diffraction peaks at $2\theta = 15.5°$, 17.1°, 23.1°, and 34.6° which represented the typical cellulose I type structure. For cellulose obtained from coconut husk, a broad peak centered at $2\theta = 22.2°$ corresponded to type III of α-cellulose [40]. A peak at 27° also indicated the presence of impurities. Similar observations were also obtained from cellulose isolated from fern fiber. XRD analysis of holocellulose isolated from coconut fiber showed the broad diffraction peak centered at 22° with a small hump appearing at 16°. A similar pattern was observed on holocellulose from fern fiber; however, the intensity was slightly lower than coconut holocellulose.

XRD analysis was also carried out on cellulose after photocatalytic reaction. It should be noted that only cotton linter cellulose can be filtered from the solution, while cellulose samples from coconut husk and fern fiber were dispersed in water, which prevented separation from the catalysts. The calculated degrees of crystallinity of cellulose before and after photocatalytic reaction were measured at 87% and 92% respectively. It is interesting to see that the crystallinity increased following H_2 production. This implied the removal of readily dissolved amorphous components, such as hemicellulose during the reaction and consequently increased the crystallinity index [30, 41, 42]. The emergence of a new peak at 25.9° was due to the presence of remaining TiO_2 catalysts that were trapped on the cellulose.

3.2.2 FTIR analysis of cellulose

Figure 5 shows the FTIR spectra of cotton linter cellulose (before and after reaction), cellulose, and holocellulose extracted from coconut husk and fern fiber. The absorption peaks around 3299 cm^{-1}, 2890 cm^{-1}, 1427 cm^{-1}, 1368 cm^{-1}, and 892 cm^{-1} for all spectra indicated the typical characteristics of cellulose I. The peaks were visible on all cellulose and holocellulose samples but at different intensities. A broad band centered at 3299 cm^{-1} was observed on cotton linter cellulose, corresponding to the stretching vibration of the hydroxyl group. The hydroxyl band appeared broader on cellulose and holocellulose from coconut husk and fern fiber, suggesting the adsorption of water on the surface. The adsorption band at ~ 2770–3000 cm^{-1} corresponded to the stretching of asymmetric and symmetric -CH groups. For cellulose and holocellulose derived from coconut and fern biomass, the CH band appeared at 2926 cm^{-1} and 2849 cm^{-1} suggesting the presence of C-H band attached to a different environment. A well-defined absorption band around 1629 cm^{-1} in cellulose samples extracted from coconut husk and fern fiber was ascribed to OH bending of the adsorbed water, but the intensity

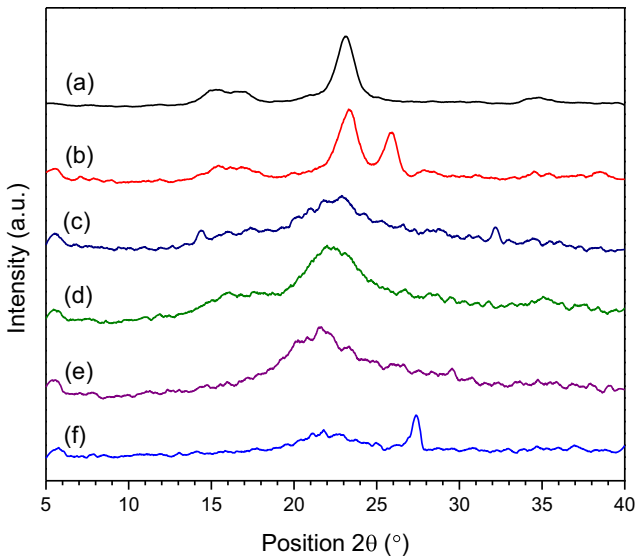

Fig. 4 XRD patterns of (a) cotton linter cellulose, (b) cotton linter cellulose (after photocatalytic reaction), (c) fern fiber holocellulose, (d) coconut husk holocellulose, (e) fern fiber cellulose, (f) coconut husk cellulose

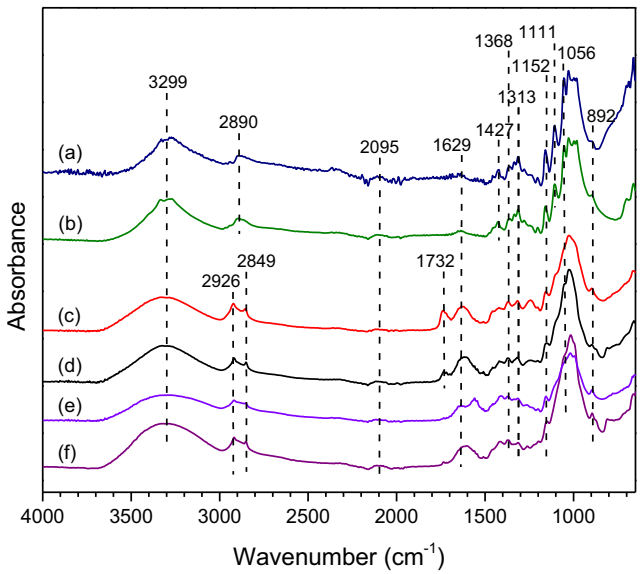

Fig. 5 FTIR spectra of (a) cotton linter cellulose (before reaction), (b) cotton linter cellulose (post-reaction), (c) coconut husk holocellulose, (d) fern fiber holocellulose, (e) coconut husk holocellulose, (f) fern fiber cellulose

of the band was reduced in cotton linter cellulose. The adsorption band situated at 1427 cm^{-1} was due to the -CH_2 bending. The bending vibration peak detected at 1313 cm^{-1} was associated with the C-H and the C-O bonds in the polysaccharide aromatic rings. A small absorption peak at 1111 cm^{-1} was attributed to the bending of the OH group. C-O-C stretching vibrations of skeletal glucose rings and pyranose were located at 1152 cm^{-1} and 1056 cm^{-1} respectively. However, the peak intensities were visibly reduced for cellulose isolated from coconut and fern fibers. The stretching vibrations [n(CO)] of the COOOC glycosidic bridge appearing in 1175–1140 and 1000–970 cm^{-1} ranges were attributed to the difference in the glycosidic linkage configuration [43]. A small absorption band at 892 cm^{-1} corresponded to the cellulosic β-glycosidic linkages that consist of C1-H and O-H bending between glucose unit in cellulose [30, 41, 42, 44, 45]. There were no significant differences of the infrared spectra between cotton linter cellulose before and after photocatalysis reaction. However, the adsorption band at ~660 cm^{-1} that corresponded to the hydroxyl group out-of-plane bending gained more intensity after the reaction, which may indicate the presence of hydrolyzed fragments of cellulose [46]. Holocellulose extracted from coconut husk and fern fibers showed the characteristic bands of hemicellulose at 1732 cm^{-1}, which corresponded to the C=O adsorption band of the acetyl group in hemicellulose [47].

3.2.3 FESEM analysis of cellulose

Cotton linter cellulose was analyzed using SEM to investigate the morphology changes after photocatalytic reaction. Figure 6(a) showed a long rod-like shape morphology with smooth surface which was a typical structure of cotton linter cellulose. The cellulose fibril surface was reported to have non-fibrous components, e.g., lignin and hemicellulose, that were bound together to form a thick and smooth coating protecting the cellulose [30, 41]. After hydrolysis, the smooth surface of cellulose fiber was partially damaged, resulting in a corrugated texture. Although the rod-like shape structure remained unchanged, the corrugated surface indicated the removal of surface coating for further decomposition of cellulose to hydrogen gas [30].

3.3 Photocatalytic H_2 production

3.3.1 Effect of metal co-catalysts on H_2 production

Photocatalytic hydrogen production from cellulose cotton linter using different types of metal co-catalysts (0.3% Pd, 0.3% Cu, 0.3%Ce, and 0.3% Ni) was investigated as shown in Fig. 7(a). No hydrogen was detected when the reaction was carried out without the presence of catalysts, indicating that cellulose did not self-decompose under light to generate hydrogen gas. Negligible hydrogen was also observed when the reaction was carried out in a dark environment, eliminating the possibility of H_2 produced from mechanocatalysis reaction. Photodecomposition using TiO_2 as catalysts only showed trace amounts of hydrogen, which indicated the importance of metals as co-catalyst to drive photocatalytic reaction. Pd/TiO_2 appeared to be the most active catalyst, producing 131 μmol of H_2 followed by Cu/TiO_2 at 50 μmol in 3 h. However, not all metal co-catalysts enhanced the photocatalytic performance of TiO_2; Ni/TiO_2 and Ce/TiO_2 only produced a very small amount of hydrogen over 3 h. Ce/TiO_2 only started to produce hydrogen after 90 min and the rate increased to give ~10 μmol whereas for Ni/TiO_2, only small traces of hydrogen were detected.

Since Pd generated high H_2 yield from cellulose, the effect of metal loading was carried out using Pd/TiO_2 at 0.3%, 0.05%, and 0.03% in order to minimize the amount of expensive Pd metal used as co-catalysts (Fig. 7(b)). The reaction was carried out for 3 h and the rate of hydrogen production

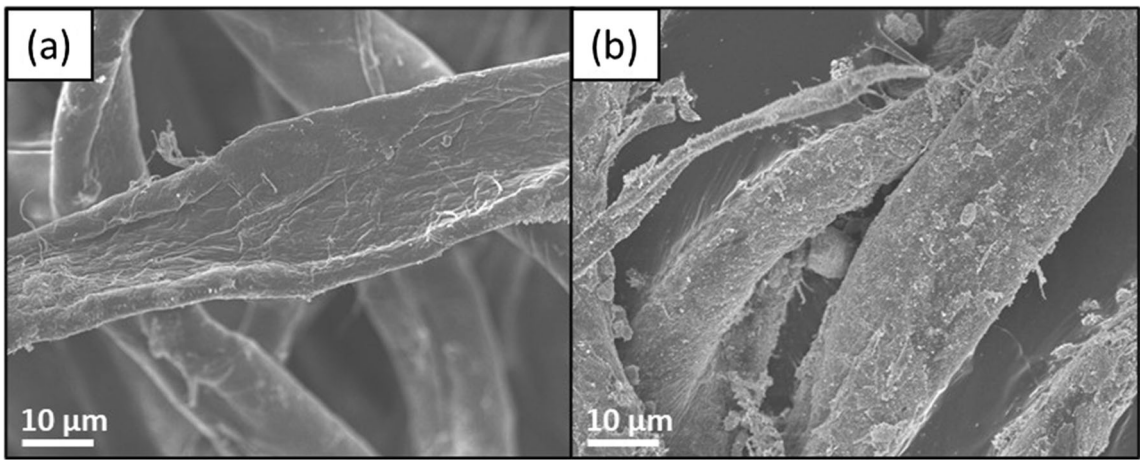

Fig. 6 SEM images of cotton linter cellulose (a) before photocatalysis and (b) after photocatalysis

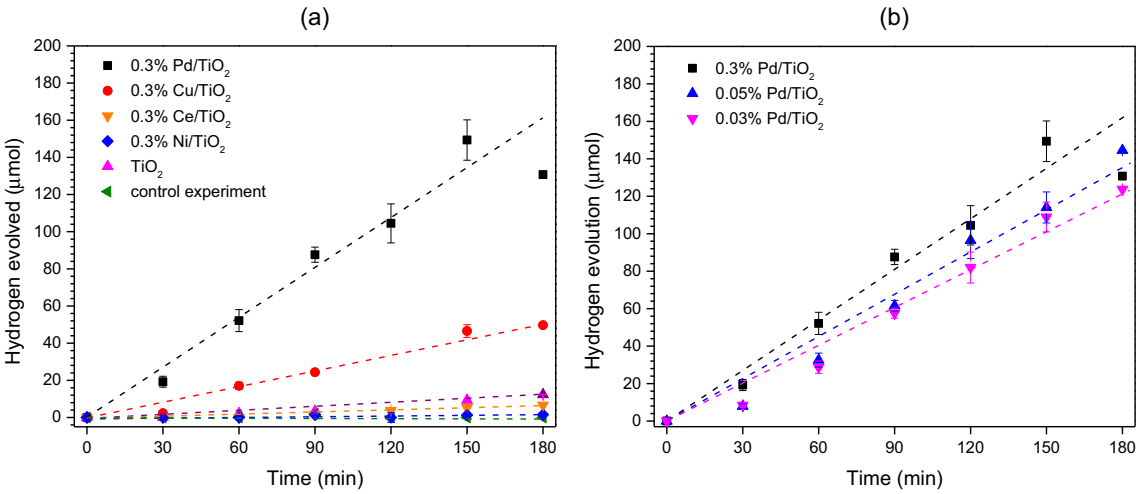

Fig. 7 (a) H_2 production from direct photocatalytic degradation of cellulose using 0.3% metal/TiO_2 catalysts in comparison to TiO_2. (b) H_2 production from photodecomposition of cellulose as a function of time over Pd/TiO_2 at different metal loading

showed no significant reduction despite Pd content being reduced from 0.3% to 0.03%. The presence of highly dispersed Pd nanoparticles on TiO_2 surface increased the number of active sites for H_2; however, high Pd loading caused particle size agglomeration that reduced the rate of H_2 production [48]. We suggest that at low Pd loading ~ 0.03%, particle agglomeration was less likely to occur. A similar number of active sites were produced despite different amounts of metal loading, hence resulting in no detrimental effect on the H_2 production. The amount of hydrogen produced at 0.03% of Pd loading was also significantly higher in comparison to TiO_2 alone. The results suggested that although Pd is considered a precious metal that contributed to the high operational cost of catalyst production, the use of only 0.03% Pd is practical and cost-effective in producing relatively large amounts of hydrogen.

3.3.2 H_2 production from cellulose cotton linter, coconut husk, and fern fiber on Pd/TiO_2

Decomposition of cellulose for H_2 production was carried out using cotton linter cellulose, and cellulose isolated from raw biomass wastes (coconut husk and fern fiber) on 0.3% Pd/TiO_2. Figure 8(a) showed a high rate of hydrogen production at ~ 130 µmol when using cellulose cotton linter. Cellulose from coconut fiber produced 38 µmol of H_2, which indicated significant reduction of H_2 yield when compared to cotton linter cellulose. Hydrogen production evolved from fern-derived cellulose occurred at a much slower rate to give 6 µmol of H_2 in 3 h. The results demonstrated the potential use of cellulose from natural biomass resources as a sustainable feedstock for hydrogen production via photocatalysis. The level of H_2 production also varied depending on the type of biomass used for cellulose isolation.

Holocellulose isolated from coconut husk and fern fiber was then used for H_2 production on 0.3% Pd/TiO_2. As can be seen in Table 1, high production of H_2 gas was observed on both holocellulose isolated from coconut husk and fern fiber in comparison to their respective cellulose counterparts. After 3 h of photocatalytic reaction, ~ 65 µmol of H_2 was measured from coconut holocellulose, which was almost double the H_2 produced from coconut cellulose (~ 38 µmol). For holocellulose isolated from fern fiber, significant H_2 production was also observed at 24 µmol, which is almost four times higher than the corresponding cellulose. Holocellulose was extracted from biomass waste containing high hemicellulose fractions (Table 1), and therefore, high H_2 production observed from holocellulose suggested that hemicellulose could enhance H_2 production.

Hydrogen production at different cellulose concentrations was carried out to investigate the dependency of hydrogen production on the amount of cellulose (Fig. 8(b)). Cellulose cotton linter was varied between 5 and 100 mg, which showed the rate of H_2 production increased with the amount of cellulose. The presence of cellulose was crucial to scavenge the photogenerated hole. The irreversible reaction between cellulose and the hole generated in the valence band of TiO_2 improved the separation of charge carriers during photocatalytic excitation, resulting in efficient electron and hole separation. Apart from the role as a sacrificial agent that inhibited the recombination of photogenerated electron-hole pairs [49], cellulose also simultaneously acted as a reactant for generation of hydrogen [26] [50]. Higher cellulose concentrations increased the amount of available substrates for decomposition, which resulted in a higher photocatalytic performance.

3.3.3 H_2 production from sugar derived from hydrothermal treatment of cellulose

Cellulose is a polymeric biomaterial consisting of sugar monomers such as sucrose and glucose. High-pressure and high-temperature conditions via hydrothermal treatment were

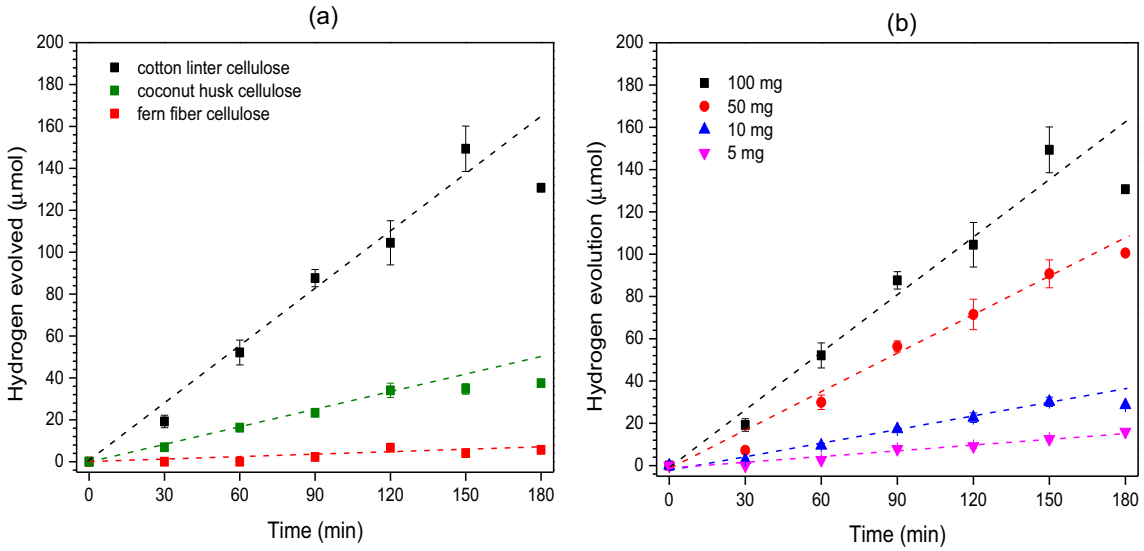

Fig. 8 (a) H_2 production from photodecomposition of cellulose from cotton linter, coconut husk, and fern fiber using 0.3% Pd/TiO_2. (b) H_2 production from photodecomposition of cellulose at different concentrations as a function of time over 0.3% Pd/TiO_2

employed to disintegrate cellulose into aqueous sugar mixtures. GC-MS analysis of the aqueous solution recovered after 35 min of cellulose hydrothermal treatment showed the presence of a mixture of glucose and fructose. Cellulose in its natural form was stable towards decomposition. Only 6.8% of cellulose converted to monosaccharides at 250 °C, with 91.1% selectivity towards glucose, and 8.8% selectivity towards fructose. Aqueous solution containing glucose and fructose was subsequently used for photocatalytic H_2 production (Fig. 9). A control experiment carried out in the absence of a photocatalyst showed only trace amounts of hydrogen produced. The photocatalytic activity for Pd/TiO_2, Cu/TiO_2, and TiO_2 for 3 h under light illumination exhibited significantly higher H_2 production from cellulose cotton linter. It is interesting to note that Cu/TiO_2 was active for hydrogen production from glucose and sucrose to give ~ 100 µmol of H_2, in comparison to reaction with cellulose at only ~ 10 µmol of H_2.

4 Discussion

Cellulose are lignocellulosic materials with polysaccharide chains that can be utilized as renewable feedstocks for H_2 production via photocatalytic decomposition. Pd/TiO_2 was found to be the most active catalyst for H_2 followed by Cu/TiO_2, Ce/TiO_2, and Ni/TiO_2. Reducing the Pd loading to only 0.03 wt.% showed no significant reduction in the H_2 production and therefore can mitigate the concern associated with the cost of Pd as an expensive metal. The photocatalytic activity of the catalysts was found to depend on the reducibility of metals in the photocatalytic environment. $Metal/TiO_2$ photocatalysts were calcined at 550 °C and therefore oxidized into metal oxides. PdO was photoreduced under UV irradiation to form Pd^o, which can then accept the photogenerated electron from TiO_2 [39]. In contrast, NiO, CuO, and CeO were stable towards photoreduction and existed in various oxidation states. Another plausible explanation of the high activity of Pd/TiO_2 was the formation of Schottky barrier. At the metal-TiO_2 interface, a Schottky barrier formed when the work functions of the metal were greater than that of TiO_2. The presence of this barrier minimized the electron-hole recombination upon photoexcitation, resulting in prolonged charge carriers' lifetime and greatly enhancing the photocatalytic performance [28]. The work functions of Pd and Cu were 5.12 eV and 4.65 eV respectively, both of which were relatively higher than TiO_2 (4.2 eV) [51]. This implied that Pd has a larger work function that increased the Schottky barrier effect.

Table 1 The properties of cellulose of cotton linter, coconut husk, and fern fiber and the amount of H_2 produced within 3 h using 0.3% Pd/TiO_2 catalysts

Biomass	Biomass sources	α-Cellulose, %	Hemicellulose, %	DP	CI, %	H_2 yield, µmol
Cellulose	Cotton linter	98.9	0.50	176	87	131 ± 0.04
Cellulose	Coconut husk	96.4	3.6	77	45	38 ± 0.01
Holocellulose		76.8	23.2	95	57	65 ± 0.02
Cellulose	Fern fiber	73.1	26.9	90	42	6 ± 0.00
Holocellulose		66.0	34.0	81	59	24 ± 0.01

DP, degree of polymerization; *CI*, crystallinity index

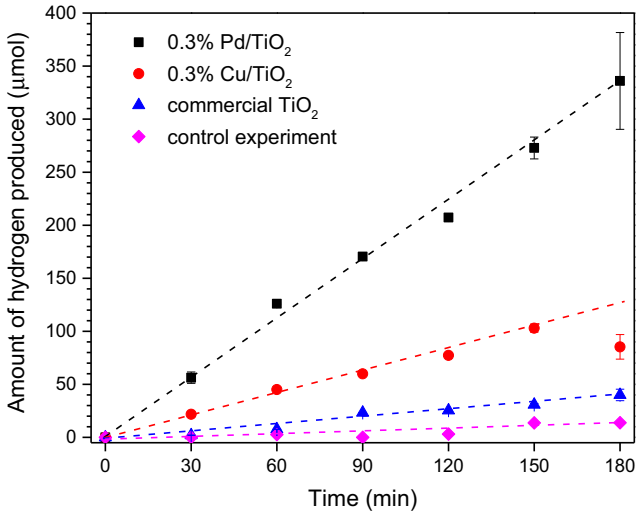

Fig. 9 H_2 production from the aqueous solution containing glucose and fructose derived from hydrothermal treatment of cellulose using TiO_2, 0.3% Pd/TiO_2, and 0.3% Cu/TiO_2

Significant amounts of hydrogen evolved from cellulose were observed despite having no pre-treatment procedures carried out in order to improve the solubility prior to the photocatalytic reaction. Cellulose is insoluble in water, which is attributed to its rigid long chain structure with strong hydrogen bonds that gives cellulose its unique strength and stability [50]. The presence of numerous hydroxyl groups in cellulose and the β-1,4-glycosidic bonds form intra- and intermolecular hydrogen bonds which resulted in stability and insolubility [52]. Pd/TiO_2 photocatalysts facilitated the process of breaking down cellulose via generation of active hydroxyl radicals. Active hydroxyl radicals dissociated the β-1,4-glycosidic bonds in cellulose into monosaccharides, followed by subsequent decomposition into H_2 and CO_2 [16]. H_2 produced from cellulose cotton linter and coconut husk in this study were comparable with the H_2 yield obtained when using Pt/TiO_2 as summarized in Table 2 [53]. To determine the viability of photocatalysis as a sustainable method for biohydrogen production, the hydrogen yields obtained from photocatalysis were compared with hydrogen yields from dark fermentation. Dark fermentation was carried out using bacterial microorganisms for fermentation of biomass substrates to biohydrogen in the absence of light [57]. The rate of hydrogen production for every gram of biomass via photocatalytic reaction was relatively higher compared to H_2 produced from dark fermentation method (Table 2). Dark fermentation required a long fermentation time for decomposition of cellulose to H_2, whereas the presence of a catalyst in a photocatalytic system accelerated the decomposition of cellulose. Our results demonstrated that biohydrogen production from lignocellulosic biomass via photocatalysis is an efficient and green process for energy generation.

Photodecomposition of cellulose at ambient conditions is an uphill reaction due to the stability of the glycosidic bonds. Thermodynamic analysis of cellulosic depolymerization via hydrolysis indicated that large concentrations of glucose were obtained from amorphous cellulose at equilibrium compared to crystalline cellulose [52]. Studies on enzymatic conversion of cellulose to glucose indicated the importance of reducing cellulose crystallinity in order to increase the glycosidic bond accessibility towards dissociation, which can occur via rearrangement of hydrogen bonding [58]. It is interesting to note that in our studies, cellulose from cotton linter with high crystallinity showed a higher rate of H_2 production than cellulose isolated from coconut husk and fern fiber. However direct comparison between the cellulose samples was not ideal since the celluloses were obtained from different sources of biomass waste. Cellulose obtained from coconut husk and fern fiber exhibited a lower degree of polymerization in comparison to cotton linter cellulose. The differences of polysaccharide units have affected the volume of H_2 production as given in Table 1. [5]. Holocellulose from coconut husk and fern fibers produced high yield of H_2 due to the presence of hemicellulose. Hemicellulose is an amorphous polysaccharide comprised of different monomeric units with acetyl groups originally linked to the xylose unit [59]. The presence of hemicellulose was suggested to enhance the hydrolysis of cellulosic materials due to the elimination of acetic acid that further accelerated β-1,4-glycosidic bond dissociation [60]. High H_2 production from glucose and fructose mixtures derived from hydrothermal treatment of cotton linter cellulose implied the rate determining step of the

Table 2 Comparison of reported H_2 production from cellulose derived from different biomass substrates via dark fermentation method with present work

Biomass sources	Biomass	Method	H_2 yield	Ref
Cotton linter	Cellulose	Photocatalysis	0.436 $mmol h^{-1} g^{-1}$	This work
Coconut husk	Cellulose	Photocatalysis	0.125 $mmol h^{-1} g^{-1}$	This work
Cotton linter	Cellulose	Photocatalysis	0.132 $mmol h^{-1} g^{-1}$	[53]
Cotton stalk	Lignocellulose	Dark fermentation	0.044 $mmol h^{-1} g^{-1}$	[54]
Cotton boll	Lignocellulose	Dark fermentation	0.032 $mmol h^{-1} g^{-1}$	[55]
Cassava residues	Cellulose	Dark fermentation	0.011 $mmol h^{-1} g^{-1}$	[10]
Sugarcane bagasse	Cellulose	Dark fermentation	0.046 $mmol h^{-1} g^{-1}$	[56]

reaction may be the dissociation of β-1,4-glycosidic bonds. H_2 production from glucose was initiated by OH radicals to form gluconic acid, which subsequently underwent further decarboxylation to form H_2 and CO_2 gasses [61].

5 Conclusion

Photocatalytic decomposition of cellulose extracted from biomass waste for H_2 production demonstrated the feasibility of harvesting raw biomass for sustainable production of hydrogen. High activity of Pd/TiO_2 compared to Cu/TiO_2, Ni/TiO_2, and Ce/TiO_2 indicated the important role of metal co-catalysts to decompose cellulose into H_2. The efficiency of H_2 generation also depended on the crystallinity and the degree of polymerization of cellulose. Holocellulose extracted from coconut husk and fern fiber was more susceptible towards H_2 generation due to the release of acetic acid from hemicellulose, which accelerated hydrolysis. Aqueous solution containing glucose and fructose from hydrothermal treatment of cellulose generated a large volume of H_2 at 350 μmol in comparison to 130 μmol from direct photodecomposition of cellulose, suggesting dissociation of glycosidic bond in cellulose as the rate determining step of the reaction.

Supplementary Information The online version contains supplementary material available at https://doi.org/10.1007/s13399-020-01164-4.

Funding The authors would like to acknowledge UBD University Research Grant (UBD/RSCH/URC/RG(b)/2019/012) and Ministry of Education Brunei Darussalam scholarship to S. Abdul Razak.

References

1. Farhat W, Venditti RA, Hubbe M, Taha M, Becquart F, Ayoub A (2017) A review of water-resistant hemicellulose-based materials: processing and applications. ChemSusChem 10(2):305–323. https://doi.org/10.1002/cssc.201601047
2. Piras CC, Fernández-Prieto S, De Borggraeve WM (2019) Ball milling: a green technology for the preparation and functionalisation of nanocellulose derivatives. Nanoscale Adv 1(3):937–947. https://doi.org/10.1039/c8na00238j
3. Kanafi NM, Rahman NA, Rosdi NH, Bahruji H, Maarof H (2019) Hydrogel nanofibers from carboxymethyl sago pulp and its controlled release studies as a methylene blue drug carrier. Fibers 7(6):1–16. https://doi.org/10.3390/fib7060056
4. Onda A, Ochi T, Yanagisawa K (2009) Hydrolysis of cellulose selectively into glucose over sulfonated activated-carbon catalyst under hydrothermal conditions. Top Catal 52(6–7):801–807. https://doi.org/10.1007/s11244-009-9237-x
5. Huang YB, Fu Y (2013) Hydrolysis of cellulose to glucose by solid acid catalysts. Green Chem 15(5):1095–1111. https://doi.org/10.1039/c3gc40136g
6. Gagić T, Perva-Uzunalić A, Knez Ž, Škerget M (2018) Hydrothermal degradation of cellulose at temperature from 200 to 300 °c. Ind Eng Chem Res 57(18):6576–6584. https://doi.org/10.1021/acs.iecr.8b00332
7. Uddin MN, Daud WMAW, Abbas HF (2014) Effects of pyrolysis parameters on hydrogen formations from biomass: a review. RSC Adv 4(21):10467–10490. https://doi.org/10.1039/c3ra43972k
8. Akubo K, Nahil MA, Williams PT (2019) Pyrolysis-catalytic steam reforming of agricultural biomass wastes and biomass components for production of hydrogen/syngas. J Energy Inst 92(6):1987–1996. https://doi.org/10.1016/j.joei.2018.10.013
9. Bradbury AGW, Sakai Y, Shafizadeh F (1979) A kinetic model for pyrolysis of cellulose. J Appl Polym Sci 23(11):3271–3280. https://doi.org/10.1002/app.1979.070231112
10. Zhang L, Li Y, Liu X, Ren N, Ding J (2019) Lignocellulosic hydrogen production using dark fermentation by Clostridium lentocellum strain Cel10 newly isolated from Ailuropoda melanoleuca excrement. RSC Adv 9(20):11179–11185. https://doi.org/10.1039/C9RA01158G
11. Sarangi PK, Nanda S (2020) Biohydrogen production through dark fermentation. Chem Eng Technol 43(4):601–612. https://doi.org/10.1002/ceat.201900452
12. Zou J, Zhang G, Xu X (2018) One-pot photoreforming of cellulosic biomass waste to hydrogen by merging photocatalysis with acid hydrolysis. Appl Catal A Gen 563(March):73–79. https://doi.org/10.1016/j.apcata.2018.06.030
13. Zhang L, Wang W, Zeng S, Su Y, Hao H (2018) Enhanced H2 evolution from photocatalytic cellulose conversion based on graphitic carbon layers on TiO2/NiOx. Green Chem 20(13):3008–3013. https://doi.org/10.1039/c8gc01398e
14. Ito M, Hori T, Teranishi S, Nagao M, Hibino T (2018) Intermediate-temperature electrolysis of energy grass Miscanthus sinensis for sustainable hydrogen production. Sci Rep 8(1):1–9. https://doi.org/10.1038/s41598-018-34544-y
15. Liu W, Cui Y, Du X, Zhang Z, Chao Z, Deng Y (2016) High efficiency hydrogen evolution from native biomass electrolysis. Energy Environ Sci 9(2):467–472. https://doi.org/10.1039/c5ee03019f
16. Paajanen A, Vaari J (2017) High-temperature decomposition of the cellulose molecule: a stochastic molecular dynamics study. Cellulose 24(7):2713–2725. https://doi.org/10.1007/s10570-017-1325-7
17. Mu D, Liu H, Lin W, Shukla P, Luo J (2020) Simultaneous biohydrogen production from dark fermentation of duckweed and waste utilization for microalgal lipid production. Bioresour Technol 302:122879. https://doi.org/10.1016/j.biortech.2020.122879
18. Mandeep, Kumar Gupta G, Shukla P (2020) Insights into the resources generation from pulp and paper industry wastes: challenges, perspectives and innovations. Bioresour Technol 297(November 2019):122496. https://doi.org/10.1016/j.biortech.2019.122496
19. Srivastava N, Srivastava M, Malhotra BD, Gupta VK, Ramteke PW, Silva RN, Shukla P, Dubey KK, Mishra PK (2019) Nanoengineered cellulosic biohydrogen production via dark fermentation: a novel approach. Biotechnol Adv 37(6). https://doi.org/10.1016/j.biotechadv.2019.04.006
20. Hibino T, Kobayashi K, Ito M, Ma Q, Nagao M, Fukui M, Teranishi S (2018) Efficient hydrogen production by direct electrolysis of waste biomass at intermediate temperatures. ACS Sustain Chem Eng 6(7):9360–9368. https://doi.org/10.1021/acssuschemeng.8b01701
21. Bahruji H, Maarof H, Abdul Rahman N (2019) Quantum efficiency of Pd/TiO2 catalyst for photocatalytic reforming of methanol in ultra violet region. Chem Pap 73(11):2707–2714. https://doi.org/10.1007/s11696-019-00822-w

22. Bolton JR, Strickler SJ, Connolly JS (1985) Limiting and realizable efficiencies of solar photolysis of water. Nature 316(6028):495–500. https://doi.org/10.1038/316495a0
23. Zhang G, Ni C, Huang X, Welgamage A, Lawton LA, Robertson PKJ, Irvine JTS (2016) Simultaneous cellulose conversion and hydrogen production assisted by cellulose decomposition under UV-light photocatalysis. Chem Commun 52(8):1673–1676. https://doi.org/10.1039/c5cc09075j
24. Zhao H, Kwak JH, Wang Y, Franz JA, White JM, Holladay JE (2006) Effects of crystallinity on dilute acid hydrolysis of cellulose by cellulose ball-milling study. Energy Fuel 20(2):807–811. https://doi.org/10.1021/ef050319a
25. Bahruji H, Bowker M, Davies PR, Pedrono F (2011) New insights into the mechanism of photocatalytic reforming on Pd/TiO2. Appl Catal B Environ 107(1–2):205–209. https://doi.org/10.1016/j.apcatb.2011.07.015
26. Caravaca, A., Jones, W., Hardacre, C., & Bowker, M. (2016). H2 production by the photocatalytic reforming of cellulose and raw biomass using Ni, Pd, Pt and Au on titania. Proceedings of the Royal Society A: Mathematical, Physical and Engineering Sciences, 472(2191). https://doi.org/10.1098/rspa.2016.0054
27. Kennedy J, Bahruji H, Bowker M, Davies PR, Bouleghlimat E, Issarapanacheewin S (2018) Hydrogen generation by photocatalytic reforming of potential biofuels: Polyols, cyclic alcohols, and saccharides. J Photochem Photobiol A Chem 356:451–456. https://doi.org/10.1016/j.jphotochem.2018.01.031
28. Fu X, Long J, Wang X, Leung DYC, Ding Z, Wu L, Zhang Z, Li Z, Fu X (2008) Photocatalytic reforming of biomass: a systematic study of hydrogen evolution from glucose solution. Int J Hydrog Energy 33(22):6484–6491. https://doi.org/10.1016/j.ijhydene.2008.07.068
29. Bowker M, Morton C, Kennedy J, Bahruji H, Greves J, Jones W, Davies PR, Brookes C, Wells PP, Dimitratos N (2014) Hydrogen production by photoreforming of biofuels using Au, Pd and Au-Pd/TiO2photocatalysts. J Catal 310:10–15. https://doi.org/10.1016/j.jcat.2013.04.005
30. Rahimi Kord Sofla M, Brown RJ, Tsuzuki T, Rainey TJ (2016) A comparison of cellulose nanocrystals and cellulose nanofibres extracted from bagasse using acid and ball milling methods. Adv Nat Sci Nanosci Nanotechnol 7(3). https://doi.org/10.1088/2043-6262/7/3/035004
31. Ouyang X, Wang W, Yuan Q, Li S, Zhang Q, Zhao P (2015) Improvement of lignin yield and purity from corncob in the presence of steam explosion and liquid hot pressured alcohol. RSC Adv 5(76):61650–61656. https://doi.org/10.1039/c5ra12452b
32. Carrier M, Loppinet-Serani A, Denux D, Lasnier JM, Ham-Pichavant F, Cansell F, Aymonier C (2011) Thermogravimetric analysis as a new method to determine the lignocellulosic composition of biomass. Biomass Bioenergy 35(1):298–307. https://doi.org/10.1016/j.biombioe.2010.08.067
33. Ona T, Sonoda T, Shibata M, Fukazawa K (1995) Small-scale method to determine the content of wood components from multiple eucalypt samples. TAPPI J 78(3):121–126
34. Tappi (2011). Lignin in Wood and Pulp. *T222 Om-02*, 1–7. https://doi.org/10.1023/a:1019003230537
35. Guay D (2013) Viscosity of pulp (capillary viscometer method) (revision of T 230 om-08). Tappi Standard, T 230:1–39
36. Wang J, Yu J, Zhu X, Kong XZ (2012) Preparation of hollow TiO2 nanoparticles through TiO2 deposition on polystyrene latex particles and characterizations of their structure and photocatalytic activity. Nanoscale Res Lett 7:1–8. https://doi.org/10.1186/1556-276X-7-646
37. Kwak BS, Chae J, Kim J, Kang M (2009) Enhanced hydrogen production from methanol / water photo-splitting in TiO 2 including Pd component. Bull Kor Chem Soc 30(5):0253–2964
38. Montoya AT, Gillan EG (2018) Enhanced Photocatalytic hydrogen evolution from transition-metal surface-modified TiO2. ACS Omega 3(3):2947–2955. https://doi.org/10.1021/acsomega.7b02021
39. Bahruji H, Bowker M, Davies PR, Kennedy J, Morgan DJ (2015) The importance of metal reducibility for the photoreforming of methanol on transition metal-TiO2photocatalysts and the use of non-precious metals. Int J Hydrog Energy 40(3):1465–1471. https://doi.org/10.1016/j.ijhydene.2014.11.097
40. Gong J, Li J, Xu J, Xiang Z, Mo L (2017) Research on cellulose nanocrystals produced from cellulose sources with various polymorphs. RSC Adv 7(53):33486–33493. https://doi.org/10.1039/c7ra06222b
41. Mohtar SS, Tengku Malim Busu TNZ, Md Noor AM, Shaari N, Mat H (2017) An ionic liquid treatment and fractionation of cellulose, hemicellulose and lignin from oil palm empty fruit bunch. Carbohydr Polym 166:291–299. https://doi.org/10.1016/j.carbpol.2017.02.102
42. Kumar A, Negi YS, Choudhary V, Bhardwaj NK (2014) Characterization of cellulose nanocrystals produced by acid-hydrolysis from sugarcane bagasse as agro-waste. J Mater Phys Chem 2(1):1–8. https://doi.org/10.12691/jmpc-2-1-1
43. Nikonenko NA, Buslov DK, Sushko NI, Zhbankov RG (2000) Investigation of stretching vibrations of glycosidic linkages in disaccharides and polysaccarides with use of IR spectra deconvolution. Biopolymers Biospectroscopy Sect 57(4):257–262. https://doi.org/10.1002/1097-0282(2000)57:4<257::AID-BIP7>3.0.CO;2-3
44. Zheng Y, Fu Z, Li D, Wu M (2018) Effects of ball milling processes on the microstructure and rheological properties of microcrystalline cellulose as a sustainable polymer additive. Materials 11(7):1–13. https://doi.org/10.3390/ma11071057
45. Ling Z, Wang T, Makarem M, Santiago Cintrón M, Cheng HN, Kang X, Bacher M, Potthast A, Rosenau T, King H, Delhom CD, Nam S, Vincent Edwards J, Kim SH, Xu F, French AD (2019) Effects of ball milling on the structure of cotton cellulose. Cellulose 26(1):305–328. https://doi.org/10.1007/s10570-018-02230-x
46. Fan M, Dai D, Huang B (2012) Fourier transform infrared spectroscopy for natural fibres. Fourier Transform Mater Anal. https://doi.org/10.5772/35482
47. Liu F, Yu R, Guo M (2017) Hydrothermal carbonization of forestry residues: influence of reaction temperature on holocellulose-derived hydrochar properties. J Mater Sci 52(3):1736–1746. https://doi.org/10.1007/s10853-016-0465-8
48. Abdullah N, Bahruji H, Rogers SM, Wells PP, Catlow CRA, Bowker M (2019) Pd local structure and size correlations to the activity of Pd/TiO2 for photocatalytic reforming of methanol. Phys Chem Chem Phys 21(29):16154–16160. https://doi.org/10.1039/c9cp00826h
49. Melián EP, López CR, Santiago DE, Quesada-Cabrera R, Méndez JAO, Rodríguez JMD, Díaz OG (2016) Study of the photocatalytic activity of Pt-modified commercial for hydrogen production in the presence of common organic sacrificial agents. Appl Catal A Gen 518:189–197. https://doi.org/10.1016/j.apcata.2015.09.033
50. Speltini A, Sturini M, Dondi D, Annovazzi E, Maraschi F, Caratto V, Profumo A, Buttafava A (2014) Sunlight-promoted photocatalytic hydrogen gas evolution from water-suspended cellulose: a systematic study. Photochem Photobiol Sci 13(10):1410–1419. https://doi.org/10.1039/c4pp00128a
51. Michaelson HB, Michaelson HB (2011) The work function of the elements and its periodicity. 4729(1977):6–11. https://doi.org/10.1063/1.323539
52. Popovic M, Woodfield BF, Hansen LD (2019) Thermodynamics of hydrolysis of cellulose to glucose from 0 to 100 °C: cellulosic biofuel applications and climate change implications. J Chem

Thermodyn 128:244–250. https://doi.org/10.1016/j.jct.2018.08.006

53. Lan L, Shao Y, Jiao Y, Zhang R, Hardacre C, Fan X (2020) Systematic study of H2 production from catalytic photoreforming of cellulose over Pt catalysts supported on TiO2. Chin J Chem Eng 28(8):2084–2091. https://doi.org/10.1016/j.cjche.2020.03.030
54. Li Y, Zhang Q, Deng L, Liu Z, Jiang H, Wang F (2018) Biohydrogen production from fermentation of cotton stalk hydrolysate by Klebsiella sp. WL1316 newly isolated from wild carp (Cyprinus carpio L.) of the Tarim River basin. Appl Microbiol Biotechnol 102(9):4231–4242. https://doi.org/10.1007/s00253-018-8882-z
55. Ghasemian M, Zilouei H, Asadinezhad A (2016) Enhanced biogas and biohydrogen production from cotton plant wastes using alkaline pretreatment. Energy Fuel 30(12):10484–10493. https://doi.org/10.1021/acs.energyfuels.6b01999
56. Rabelo CABS, Soares LA, Sakamoto IK, Silva EL, Varesche MBA (2018) Optimization of hydrogen and organic acids productions with autochthonous and allochthonous bacteria from sugarcane bagasse in batch reactors. J Environ Manag 223(July):952–963. https://doi.org/10.1016/j.jenvman.2018.07.015
57. Nikolaidis P, Poullikkas A (2017) A comparative overview of hydrogen production processes. Renew Sust Energ Rev 67:597–611. https://doi.org/10.1016/j.rser.2016.09.044
58. Chundawat SPS, Bellesia G, Uppugundla N, Da Costa Sousa L, Gao D, Cheh AM, Agarwal UP, Bianchetti CM, Phillips GN, Langan P, Balan V, Gnanakaran S, Dale BE (2011) Restructuring the crystalline cellulose hydrogen bond network enhances its depolymerization rate. J Am Chem Soc 133(29):11163–11174. https://doi.org/10.1021/ja2011115
59. Chen H (2015) Lignocellulose biorefinery conversion engineering. In: Lignocellulose biorefinery engineering (Issue 1). https://doi.org/10.1016/b978-0-08-100135-6.00004-1
60. Negahdar L, Delidovich I, Palkovits R (2016) Aqueous-phase hydrolysis of cellulose and hemicelluloses over molecular acidic catalysts: insights into the kinetics and reaction mechanism. Appl Catal B Environ 184:285–298. https://doi.org/10.1016/j.apcatb.2015.11.039
61. Iervolino G, Vaiano V, Murcia JJ, Rizzo L, Ventre G, Pepe G, Campiglia P, Hidalgo MC, Navío JA, Sannino D (2016) Photocatalytic hydrogen production from degradation of glucose over fluorinated and platinized TiO2 catalysts. J Catal 339:47–56. https://doi.org/10.1016/j.jcat.2016.03.032